J Mater Sci (2008) 43:5102–5108
DOI 10.1007/s10853-008-2750-7

Synthesis and optical properties of CeO_2 nanocrystalline films grown by pulsed electron beam deposition

B. Tatar · E. D. Sam · K. Kutlu · M. Ürgen

Received: 6 December 2007 / Accepted: 22 May 2008 / Published online: 7 June 2008

Abstract The nanocrystalline cerium dioxide (CeO_2) thin films were deposited on soda lime (SLG) and Corning glass by pulsed e-beam deposition (PED) method at room temperature. The structure of the produced CeO_2 thin films was investigated by X-ray diffraction (XRD) analysis, X-ray photoelectron spectroscopy (XPS), and micro Raman spectroscopy. The surface topography of the films was examined by atomic force microscopy (AFM). Film thickness and growth morphologies were determined with FEG-SEM from the fracture cross sections. XPS studies gave a film composition composed of +4 and +3 valent cerium typical to nanocrystalline ceria structures deficient in oxygen. The ceria films were polycrystalline in nature with a lattice parameter (a) of 0.542 nm. The Raman characteristics of the source material and the films deposited were very similar in character. Raman lines for thin film and bulk CeO_2 was observed at 465 cm^{-1}. The optical properties of the CeO_2 films were deduced from reflectance and transmittance measurements at room temperature. From the optical model, the refractive index was determined as 1.8–2.7 in the photon energy interval from 3.5 to 1.25 eV. The optical indirect band gap (E_g) of CeO_2 nanocrystalline films was calculated as 2.58 eV.

B. Tatar (✉) · K. Kutlu
Faculty of Arts and Sciences, Department of Physics, Yıldız Technical University, Davutpaşa, 34220 Istanbul, Turkey
e-mail: btatar@yildiz.edu.tr

E. D. Sam · M. Ürgen
Department of Metallurgical and Materials Engineering, Istanbul Technical University, Maslak, 34469 Istanbul, Turkey

Introduction

Cerium dioxide, or ceria (CeO_2), films have been used for application in optoelectronics, electrochromics, high storage capacitor devices, UV-blocking filters, silicon on insulator structures for microelectronics, and heterogeneous catalysts [1–9]. Moreover, ceria film is a very promising material for a buffer layer for high-temperature superconductors (HTS) because of their close lattice match and similar thermal expansion coefficients [10, 11].

CeO_2 films have been prepared by several production methods such as thermal evaporation [12], electron beam evaporation [13], magnetron sputtering [14–16], pulsed laser deposition (PLD) [17, 18], ion-assisted deposition [19], spray pyrolysis [20], sol-gel [21, 22], wet chemical deposition [23], chemical vapor deposition (CVD) [24], metal-organic CVD [10], and plasma-enhanced chemical vapor deposition (PE-CVD) [25, 26]. In all of these studies it can be clearly seen that the properties of the ceria films produced show strong dependence on the deposition technology used.

Pulsed e-beam deposition (PED) technique is similar to pulsed laser deposition (PLD). PED, as an ablation-based growth technique, offers stoichiometric deposition of complex multi-component materials. However, it has several advantages compared to PLD, such as lower cost, scalability, and ability to effectively interact with all types of materials (including high band gap semiconductors, oxides, etc.) through Coulomb interactions created by charge particles, i.e., electrons. Details of the technique can be found elsewhere [27–29].

To our knowledge, until now, CeO_2 films have not been deposited by PED method. The aim of this study is to investigate the possibility of production of high-quality (with high transmittance and wide range of refractive

index) optical CeO_2 films on glass substrates by pulsed electron beam method at room temperature. Low-alkali optical glass and commercial soda lime glass (high alkali content) were used as substrate materials to test the possible effects of sodium migration that might take place during the deposition process on the properties of the ceria films.

Experimental

Cylindrical CeO_2 targets, with a diameter of 10 mm, were prepared from pure CeO_2 powder (99.99% purity) by cold pressing in a stainless steel die with a load of 15,000 kg. Corning (low-alkali glass suitable for optical coatings) microscope slides and commercial soda lime glasses (SLG) were used as substrate materials. The surface roughness of the substrates as determined from AFM measurements was 0.24 and 7 nm (RMS) for Corning and SLG, respectively. Prior to coating the substrates were ultrasonically cleaned in acetone and isopropyl alcohol.

Before starting the deposition process, deposition chamber is pumped down to a base pressure 1×10^{-5} Torr. The deposition process is conducted under an oxygen pressure of 5 mTorr. A pulsed electron beam source (PEBS 2.0 Neocera Inc) has been used to deposit CeO_2 thin films. The distances between substrate and the evaporation material, and PEB source and crucible were 100 and 3 mm, respectively. The pulsed electron source was operated at 15 kV and 8 Hz frequencies with a total number of 20,000 pulses. The deposition rate achieved for ceria films was 0.005 nm per pulse. The deposition rates were calculated from the field emission gun SEM (FEG-SEM, Jeol 7000F) images of fracture cross sections of the films. Thickness of the films was determined as 100 ± 5 nm. FEG-SEM was also used to determine the growth morphology of the films from their fracture cross sections.

The chemistry of the ceria films produced was determined by using X-ray photoelectron spectroscopy (JEOL JPS-9010) by using MgKα, X-ray source operating at 12 kV and 25 mA. The analysis area diameter and pass energy of the analyzer were 6 mm and 50 eV, respectively. No depth profiling was attempted due to the well-known reducing effect of ion beam on ceria [30, 31]. The structure of the samples was investigated using Raman Spectroscopy (Horiba Jobin Yvon Labram HR-UV Spectrometer HR800UV). The samples were excited with 632.817 nm HeNe laser (Laser power = 20 mW). The crystalline structure and phase composition of the CeO_2 film were examined by glancing angle X-ray diffraction (Philips PW 3710) using CuKα radiation (glancing angle 0.5°). The surface topography of cerium dioxide films was investigated with atomic force microscopy (Shimadzu, SPM-9500J3). The optical transmittance and reflectance characteristics were determined by using an Aquila NKD 7000V UV-Visible spectrophotometer in the wavelength range of 300–1000 nm

Results and discussion

Characterization of the nanostructure CeO_2 films

The thickness and the morphology of the films that were determined from FEG-SEM investigations on fracture cross sections showed that it was possible to grow films with a thicknesses of 100 nm with the PED deposition parameters used in this study (Fig. 1a). The backscattered electron image of the film cross sections revealed that film had a columnar, nanoporous structure with column widths varying between 50 and 80 nm (Fig. 1b). Similar structures were observed both on SLG and Corning glass substrates revealing that the substrate did not exert an appreciable influence on the columnar growth morphology of the ceria films.

The results of AFM investigations of the CeO_2 films grown on Corning glass and SLG substrates by PED at room temperature were given in Fig. 2a and b. The grains observed on both substrates were multi-sized and the surface roughness of the films measured as root mean square (RMS) were around of 1.68 nm for Corning glass and 0.81 nm for SLG. In the AFM images, large grain-like structures with sizes in the range of 60–80 nm and surrounded with grain boundary-like structures were observable. These structures are most probably the reflections of porous columnar structures on the surface that were present on the FEG-SEM-investigated cross sections (Fig. 1b). In the AFM images, within these large grains, smaller crystallites were also present with sizes varying between 5–15 nm and 10–20 nm for SLG and Corning glass, respectively. The smaller crystallite sizes observed on SLG can be attributed to the higher surface roughness of this substrate material. It is well known that increased surface roughness also results in the increase of nucleation sites, which leads to smaller crystallite sizes.

The XRD patterns of CeO_2 films which were grown on SLG and Corning glass substrates were given in Fig. 3a and b, respectively. The XRD peaks were found at $2\theta = 28.5°$, 33.1°, 47.5°, and 56.3° correspond to the reflections from {111}, {200}, {220}, and {311}. The calculated lattice parameter ($a = 0.542$ nm) of ceria obtained from XRD spectra of the films is in good agreement with standard data taken from JCPDS-ICDD data card (Data file 34-0394) for cubic ceria (Table 1). The Bragg pattern indicated that the films were composed of CeO_2 that was crystallized in the cubic structure. The

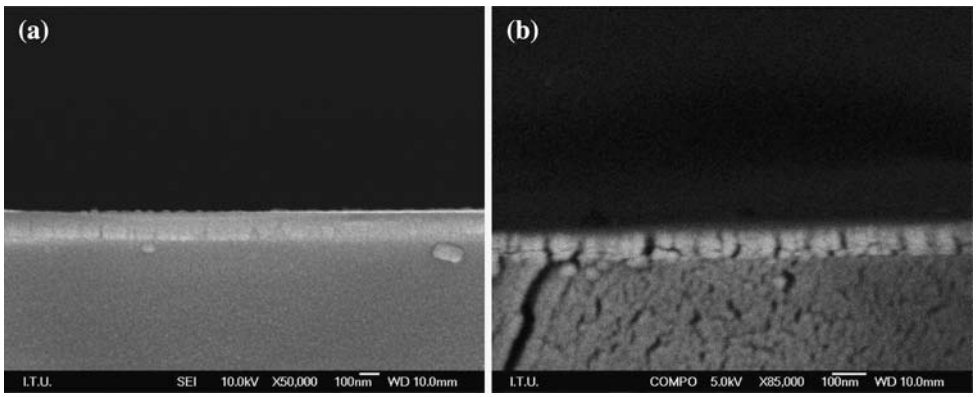

Fig. 1 The FEG-SEM images of ceria nanocrystalline films grown on Corning glass substrates: (**a**) Fracture cross-sectional image. (**b**) The backscattered electron cross-sectional image (the backscattered image is taken after a very thin layer of gold plating of the sample for achieving a better resolution)

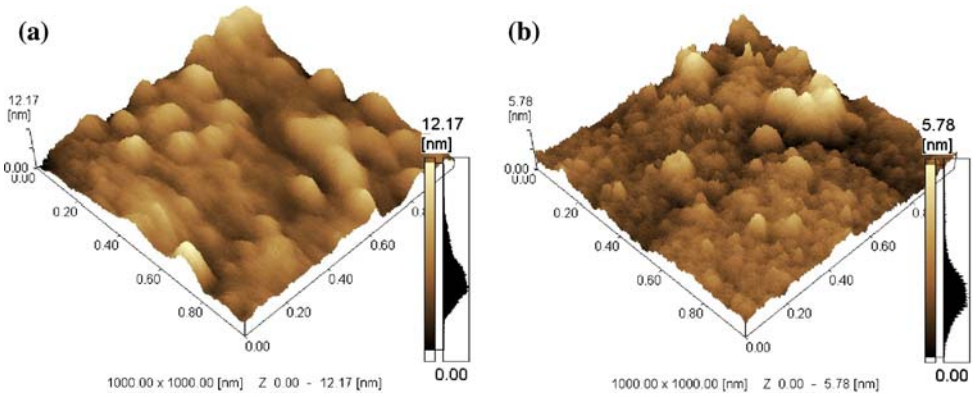

Fig. 2 The AFM images of ceria nanocrystalline films grown (**a**) on Corning glass substrates and (**b**) on SLG substrates

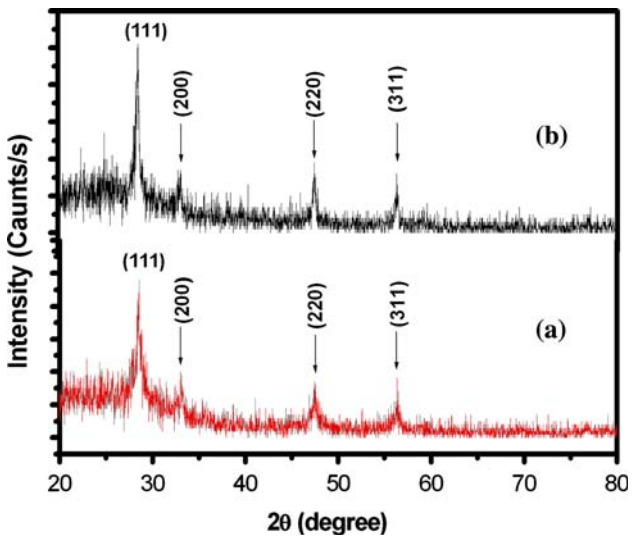

Fig. 3 XRD patterns of the PED CeO_2 nanocrystalline films: (a) on SLG substrate and (b) on Corning glass substrate

crystallite size (D_{hkl}) of CeO_2 films, which were prepared on SLG and on Corning glass substrate, was calculated using the Scherrer formula [30]. In this formula λ is the wavelength of the incident radiation, w is the Full Width of Half Maximum (FWHM) of the peak, and θ is the diffraction angle.

$$D_{hkl} = \left(\frac{0.94\lambda}{w\cos\theta}\right) \quad (1)$$

The calculated crystallite sizes of the ceria films on Corning glass and SLG, depending on orientation, varied between 7.6–22.1 nm and 9.8–14 nm, respectively (Table 1), indicating the nanocrystalline nature of the films. The average grain sizes calculated from XRD patterns and the size of crystallites observed with AFM are very close to each other. Hence these results clearly showed that it was possible to deposit crystalline ceria films without additional heating of substrates with PED.

The chemistry of the films was determined by using X-ray photoelectron spectroscopy (XPS) (Fig. 4a, b). Wide spectrum of the films showed that the film was mainly composed of cerium and oxygen, carbon arising from contamination was also present in the spectrum. In the 3d region of Ce peaks arising from both Ce^{3+} and Ce^{4+} were present. The details of the spectrum and the position of 3d5/2 and 3/2 were given in Fig. 4b and Table 2. This spectrum was almost identical to the spectrum of nanocrystalline ceria powders [31–33]. In previous studies conducted on ceria structure, it was observed that the formation of oxygen vacancies in nanocrystalline ceria went along with an increase in Ce^{3+} ion concentration and a decrease in particle size. Therefore, they concluded that the

Table 1 Standard *d* spacing values of bulk CeO_2 and calculated *d* spacings, lattice parameters, and crystallite sizes of PED-deposited ceria films

Standard '*d*' spacing value (Å)	2θ	*d* (Å)	*h k l*	*a* (nm)	Crystallite sizes (nm)	
					Corning	SLG
3.123	28.5	3.130	1 1 1	0.542	15.6	9.8
2.705	33.1	2.711	2 0 0	0.542	7.61	13.75
1.913	47.5	1.915	2 2 0	0.542	22.1	12.2
1.631	56.3	1.634	3 1 1	0.542	13.8	14

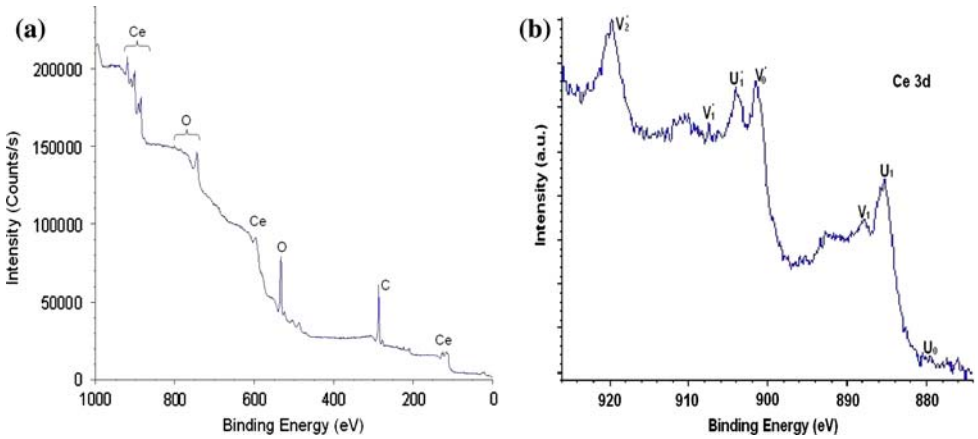

Fig. 4 XPS analysis of nanocrystalline CeO_2 films: (**a**) wide spectrum and (**b**) Ce 3d spectrum

Table 2 Assignment of Ce 3d peaks in XPS

Ce 3d 5/2				
V_0	V_1	V_2	U_0	U_1
Ce^{4+} 882.3 eV	Ce^{4+} 889 eV	Ce^{4+} 898 eV	Ce^{3+} 880.5 eV	Ce^{3+} 885.7 eV
Ce 3d 3/2				
V_0'	V_1'	V_2'	U_0'	U_1'
Ce^{4+} 901 eV	Ce^{4+} 907.5 eV	Ce^{4+} 917.5 eV	Ce^{3+} 899 eV	Ce^{3+} 904 eV

content of oxygen vacancies increased with the charge transition of $Ce^{4+} \rightarrow Ce^{3+}$ in nanocrystalline ceria structure [31–35]. These effects can be attributed to a distortion of the local symmetry arising from high surface-to-volume ratio of nanocrystalline materials and/or oxygen vacancies within the lattice.

The Raman spectra were taken at room temperature in the range of 100–1500 cm^{-1} for all samples. Figure 5a–c shows the Raman spectra of the reference CeO_2 powder, CeO_2 nanocrystalline films on Corning substrates, and SLG substrates, respectively. In the range of wave numbers investigated there is only one Raman peak located at 465 cm^{-1} which is assigned to Raman active modes (F_{2g}) for Ce-O symmetric vibrations [36–38]. This peak was clearly observed in the target material (Fig 5a). In Fig. 5b, Raman spectra of the ceria films grown on Corning glass and the substrate are given. The Raman peak at 465 cm^{-1} was also clearly observed on the coated glass. However, the Raman peak obtained from the coating was broader than the one obtained from bulk CeO_2 indicating the smaller grain size of the coating. On SLG substratesthere were a number of Raman lines making the Raman spectrum more complex (Fig. 5c). However, this complex spectrum did not obscure the Raman line from ceria coating which was clearly observable at 465 cm^{-1}. This peak was also broader than the peak of bulk CeO_2 showing the smaller crystallite size of ceria films on SLG substrate.

The results of the characterization studies showed that it was possible to produce polycrystalline and nanostructured ceria films on both Corning glass and SLG with PED technique utilized in the study. Any migration or diffusion, such as Na migration, from SLG which is an often encountered problem affecting the film quality [39, 40] was not observed due to the low temperatures used in the PED process. The only difference was the smaller crystallite sizes of the films formed on SLG resulting from higher roughness of these substrates.

Optical properties

The optical properties of semiconducting CeO_2 nanocrystal thin films were determined from transmission and reflection measurements conducted in the wavelength range of

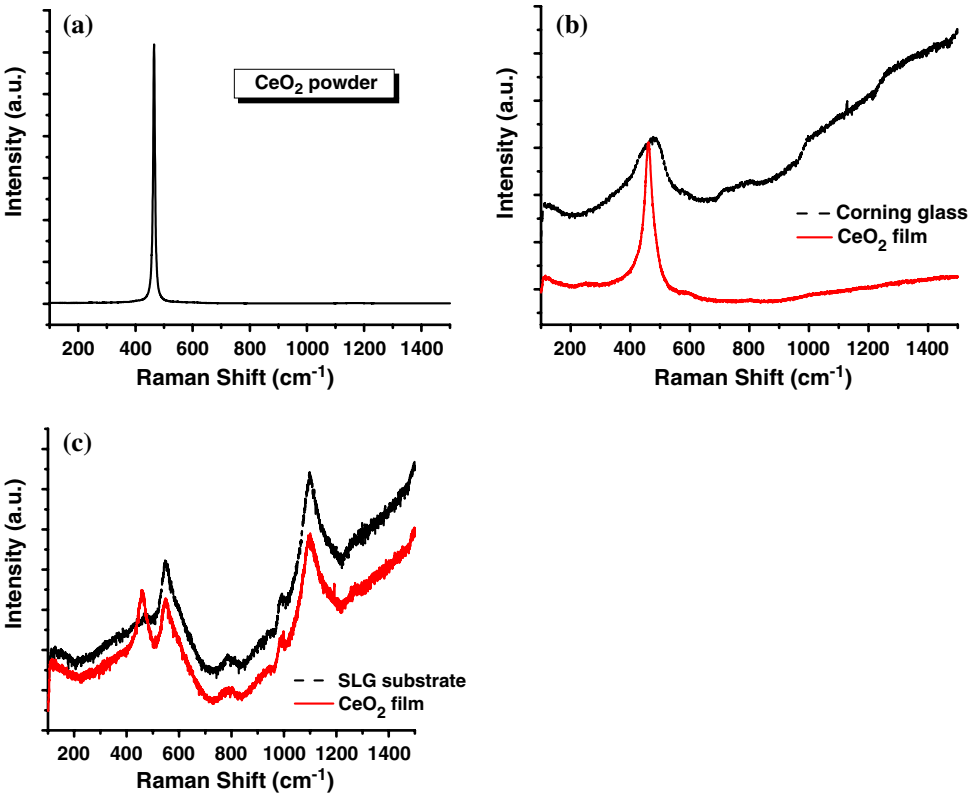

Fig. 5 Micro Raman spectra of the ceria powder and CeO_2 nanocrystalline films grown on SLG and Corning glass substrates by PED

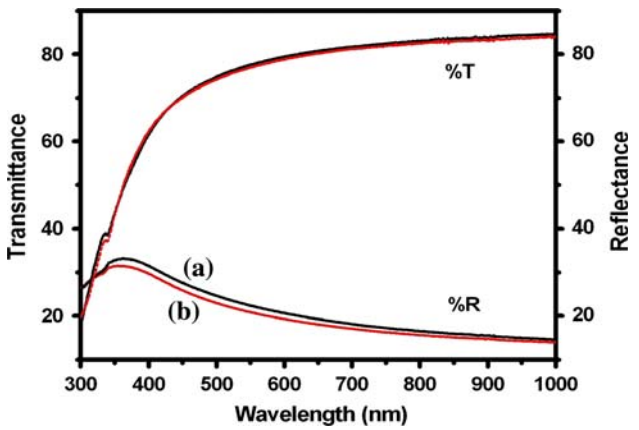

Fig. 6 The transmittance and reflectance spectrum of CeO_2 films grown (a) on Corning glass substrates and (b) on SLG substrate by PED

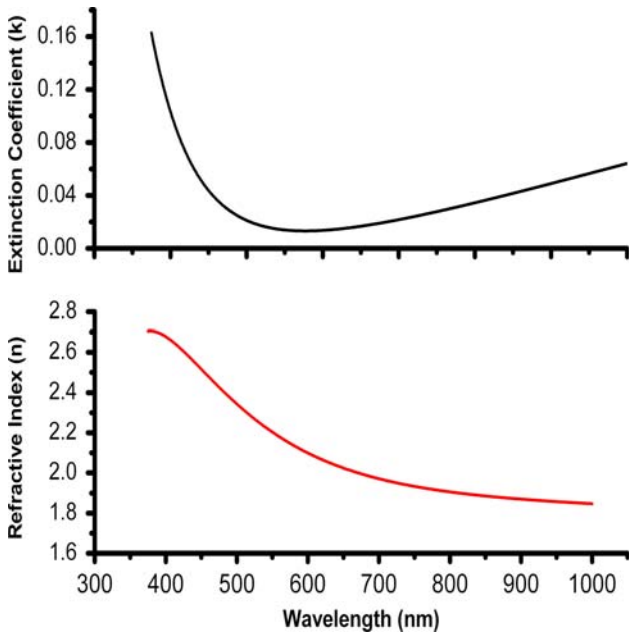

Fig. 7 Index of refraction n and extinction coefficient k vs. wavelength for CeO_2 films on Corning glass substrates

300–1000 nm at room temperature (Fig. 6a, b). Transmittance and reflectance measurements were normalized with respect to the Corning glass substrates. The sharp absorption edge for these films was around 350 nm in near-infrared region and these films exhibit a high transparency (above 80%) in visible region. The difference in the glass substrate did not exhibit any difference on the transmittance and reflectance properties. In the other optical property determinations only data collected from films deposited on Corning glass substrates were used because of their well-defined and consistent optical responses. The dispersion of the refractive index n (λ) and the extinction coefficient were calculated by fitting both reflectance and transmittance data [41, 42] and were given in Fig. 7a and b.

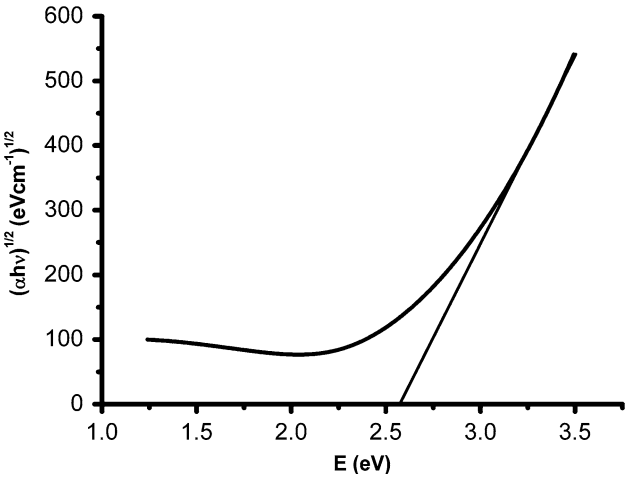

Fig. 8 Plot of the $(\alpha hv)^{1/2}$ vs. photon energy (hv) for the determination of the indirect optical band gap of CeO_2 nanocrystalline films

The refractive index and the extinction coefficients, which were calculated in the photon energy interval from 3.5 to 1.25 eV (300–1000 nm), were between 1.8–2.7 and, 0.06–0.16, respectively. The refractive index and the extinction coefficient (k) of the films at 632 nm were measured as 2.0 and 0.015, respectively.

The optical band gap E_g was determined from the absorption coefficient according to the solid band theory [39, 40]. The absorption coefficient α was calculated from k (extinction coefficient) value using $\alpha = (4\pi k/\lambda)$. The dependence of the absorption coefficient ($\alpha(hv)$), on the energy of the incoming photons (hv) is given by $\alpha(hv) = \text{constant}(hv - E_g)^2$ in the case of materials with an indirect band gap. The $(\alpha hv)^{1/2}$ vs. photon energy (hv) plot yielded a direct energy gap of 2.58 eV for ceria films used in this study (Fig. 8). The calculated indirect band gap values were lower than the band gap values of other physical vapor-deposited CeO_2 films (3–3.5 eV) [6–9]. The differences observed in the band gap values of nano- and microcrystalline ceria were attributed to the presence of increased oxygen vacancies in the nanocrystalline structure of the ceria which leads to a distortion of the local symmetry [33–35]. Normally nanocrystallinty is expected to lead blue shift effects due to quantum confinement [4, 26]. However, the red shift effect observed in the nanocrystalline ceria may be explained by the formation of localized states within the band gap owing to oxygen vacancies and increased Ce^{3+} ion concentration.

The nanocrystalline ceria films produced with PED, with their low refractive indices ($n = 1.8$–2.7), resulting in high transmittance in the visible and near IR region (over 80%), high absorbance characteristics in the UV region, and indirect optical band gap of 2.58 eV are promising for optoelectronic applications.

Conclusions

In this study, the nanocrystalline cerium dioxide (CeO_2) thin films have been successfully prepared on SLG and Corning glass by pulsed e-beam evaporation (PED) method at room temperature. The results of both XRD analysis and Raman spectroscopy showed that the synthesized CeO_2 has a cubic fluorite structure with crystallite sizes in the nanometer scale. The optical absorption in the edge region of these CeO_2 films was evaluated as $E_g = 2.58$ eV which is characteristic for an indirect transition semiconductor. The red shift creating effect of the presence Ce^{3+} (as determined from XPS measurements) and oxygen vacancies in nanocrystalline ceria is further verified. The results showed that PED can be used as an alternative technique for the production of nanocrystalline ceria films.

Acknowledgements The authors gratefully acknowledge JEOL-Japan for the valuable support they have given in XPS measurements and Dr. Gültekin Göller and H. Sezer for the FEG-SEM investigations. This study is partially supported through the "Advances Technologies in Engineering" project financed by State Planning Organization of Turkey.

References

1. Becht M, Morishita T (1996) Chem Vap Deposition 2:191. doi:10.1002/cvde.19960020508
2. Al-Robaee MS, Krishna MG, Rao KN, Mohan S (1991) J Vac Sci Technol A 9:6. doi:10.1116/1.577171
3. Schwab RG, Steiner RA, Mages G, Beie HJ (1992) Thin Solid Films 207:283. doi:10.1016/0040-6090(92)90139-3
4. Chen MY, Zu XT, Xiang X, Zhang HL (2007) Physica B (Amsterdam) 389:263. doi:10.1016/j.physb.2006.06.162
5. Zhang DE, Ni XM, Zheng HG, Zhang XJ, Song JM (2006) Solid State Sci 8:1290. doi:10.1016/j.solidstatesciences.2006.08.003
6. Kanakaraju S, Mohan S, Sood AK (1997) Thin Solid Films 305:191. doi:10.1016/S0040-6090(97)00081-3
7. Yamshita M, Kameyama K, Yabe S, Yoshida S, Fujishiro Y, Kawai T et al (2002) J Mater Sci Lett 37:683
8. Özer N (2001) Sol Energy Mater Sol Cells 68:391. doi:10.1016/S0927-0248(00)00371-8
9. Porqueras I, Person C, Corbella C, Vives M, Pinyol A, Bertran E (2003) Solid State Ionics 165:131. doi:10.1016/j.ssi.2003.08.025
10. Malandrino G, Lo Nigro R, Benelli C, Castelli F, Fragala IL (2000) Chem Vap Deposition 6:233. doi:10.1002/1521-3862(200010)6:5<233::AID-CVDE233>3.0.CO;2-D
11. Kim L, Kim J, Lee H, Jung D, Roh Y (2001) Jpn J Appl Phys 2(40):L564
12. Hass G, Ramsay JB, Thun R (1958) J Opt Soc Am 48:324
13. Baudry P, Rodrigues ACM, Aegerter M, Bulhoes LO (1990) Mater J Non-Cryst Solids 121:319. doi:10.1016/0022-3093(90)90151-B
14. Chin CC, Lin RJ, Yu YC, Wang CW, Lin EK, Tsai WC et al (1997). IEEE Trans Appl Superconduct 2:7
15. Patel M, Kim K, Ivill M, Budai JD, Norton DP (2004) Thin Solid Films 468:1. doi:10.1016/j.tsf.2004.02.105
16. Masetti E, Varsano F, Decker F, Krasilnikova A (2001) Electrochim Acta 46:2085. doi:10.1016/S0013-4686(01)00410-8

17. Hirschauer B, Chiaia G, Gothelid M, Karlsson UO (1999) Thin Solid Films 348:3. doi:10.1016/S0040-6090(98)01759-3
18. Karakaya K, Barcones B, Rittersma ZM, Van Berkum JGM, Verheijen MA, Rijinders G et al (2006) Mater Sci Semiconductor Process 9:1061
19. Koo WH, Jeoung SM, Choi SH, Jo SJ, Baik HK, Lee SJ et al (2004) Thin Solid Films 468:28. doi:10.1016/j.tsf.2004.03.042
20. Elidrissi B, Addou M, Regragui M, Monty C, Bougrine A, Kachouane A (2000) Thin Solid Films 379:23. doi:10.1016/S0040-6090(00)01404-8
21. Ghodsi FE, Tepehan FZ (2006) Phys Status Solidi A 203:526. doi:10.1002/pssa.200521309
22. Reisfeld R, Zayat M, Minti H, Zastrow A (1998) Sol Energy Mater Sol Cells 54:109. doi:10.1016/S0927-0248(98)00061-0
23. Keomany D, Pettit JP, Deroo D (1995) SPIE Proc 2255:513
24. Pollard KD, Jenkins HA, Puddephatt RJ (2000) Chem Mater 12:701. doi:10.1021/cm990455r
25. Barreca D, Gasparotto A, Tondello E, Sada C, Polizzi S, Benedetti A (2003) Chem Vap Deposition 4:9
26. Barreca D, Bruno G, Gasparotto A, Losurdo M, Tondello E (2003) Mater Sci Eng C 23:1013. doi:10.1016/j.msec.2003.09.103
27. Lee DF, Christen HM, List FA, Heatherly L, Leonard KJ, Rouleau CM, Cook SW, Martin PM, Paranthaman M, Goyal A (2005) Physica C 426–431:878
28. Guo YF, Chen LM, Lei M, Guo X, Li PG, Tang WH (2006) Physica C 450:96. doi:10.1016/j.physc.2006.08.017
29. Choudhary RJ, Ogale SB, Shinde SR, Kulkarni VN, Venkatesan T, Harshavardhan KS et al (2004) Appl Phys Lett 84:1483. doi:10.1063/1.1651326
30. Klug HP, Alexander LE (1974) X-ray diffraction procedures, 2nd edn. Wiley, New York
31. Qiu L, Liu F, Zhao L, Ma Y, Yao J (2006) Appl Surf Sci 252:4931. doi:10.1016/j.apsusc.2005.07.024
32. Zhang F, Wang P, Koberstein J, Khalid S, Chan SW (2004) Surf Sci 563:74. doi:10.1016/j.susc.2004.05.138
33. Chuang FY, Yang SM (2008) J Colloid Interface Sci 320:194. doi:10.1016/j.jcis.2008.01.015
34. Deshpande S, Patil S, Kuchibhatla S (2005) Appl Phys Lett 87:133113. doi:10.1063/1.2061873
35. Patsalas P, Logothetidis S, Metaxa C (2002) Appl Phys Lett 81:466. doi:10.1063/1.1494458
36. Weber WH, Hass KC, McBride JR (1993) Phys Rev B 48:178. doi:10.1103/PhysRevB.48.178
37. Spanier JE, Robinson RD, Zhang F, Chan SW, Herman IP (2001) Phys Rev B 64:245407. doi:10.1103/PhysRevB.64.245407
38. Siokou A, Ntais S, Dracopoulos V, Papaefthimiou S, Leftheriotis G, Yianoulis P (2006) Thin Solid Films 514:87. doi:10.1016/j.tsf.2006.02.077
39. Odo GY, Nogueira LN, Lepienski CM (1999) J Non-Cryst Solids 247:232. doi:10.1016/S0022-3093(99)00076-9
40. Ollier N, Boizot B, Reynard B, Ghaleb D, Petite G (2004) Nucl Instrum Meth Phys Res B 218:176
41. Heavens OS (1991) Optical properties of thin solid films. Dover, New York
42. Pankove JI (1971) Optical process in semiconductors. Prentice-Hall